Annular Mode–Like Variation in a Multilayer Quasigeostrophic Model

YANG ZHANG, XIU-QUN YANG, AND YU NIE

School of Atmospheric Sciences, Nanjing University, Nanjing, China

GANG CHEN

Department of Earth and Atmospheric Sciences, Cornell University, Ithaca, New York

(Manuscript received 10 August 2011, in final form 17 May 2012)

ABSTRACT

Eddy–zonal flow interactions in the annular modes are investigated in this study using a modified beta-plane multilayer quasigeostrophic (QG) channel model. This study shows the different response of high- and low-phase-speed (frequency) eddies to the zonal wind anomalies and suggests a baroclinic mechanism through which the two eddies work symbiotically maintaining the positive eddy feedback in the annular modes. Analysis also indicates that the different roles played by these two eddies in the annular modes are related to the differences in their critical line distributions. Eddies with higher phase speeds experience a low-level critical layer at the center of the jet. They drive the zonal wind anomalies associated with the annular mode but weaken the baroclinicity of the jet in the process. Lower-phase-speed eddies encounter low-level critical lines on the jet flanks. While their momentum fluxes are not as important for the jet shift, they play an important role by restoring the lower-level baroclinicity at the jet center, creating a positive feedback loop with the fast eddies that extends the persistence of the jet shift.

The importance of the lower-level baroclinicity restoration by the low-phase-speed eddies in the annular modes is further demonstrated in sensitivity runs, in which surface friction on eddies is increased to selectively damp the low-phase-speed eddies. For simulations in which the low-phase-speed eddies become inactive, the leading mode of the zonal wind variability shifts from the position fluctuation to a pulsing of the jet intensity. Further studies indicate that the response of the lower-level baroclinicity to the zonal wind anomalies caused by the low-phase-speed eddies can be crucial in maintaining the annular mode–like variations.

1. Introduction

The annular modes are the leading modes of extratropical variability of the Northern and Southern Hemisphere tropospheric winds on intraseasonal time scales. This annular pattern exhibits an equivalent barotropic dipolar structure and is often described as a zonally symmetric latitudinal shift of the midlatitude jets (e.g., Hartmann and Lo 1998; Limpasuvan and Hartmann 2000; Thompson and Wallace 2000). The observed anomalous zonal winds in the annular modes are often more persistent than baroclinic eddies (Feldstein and Lee 1998; Hartmann and Lo 1998). Multiple studies suggest that the zonal wind persistence is extended because of a positive feedback between the eddy momentum forcing and the zonal wind anomalies (Limpasuvan and Hartmann 2000; Lorenz and Hartmann 2001, 2003). As an internal mode of variability, understanding the mechanism that sustains the zonal wind anomalies is useful not only to predict the intraseasonal variability in the extratropics but also for climate change projections. As suggested in Ring and Plumb (2007, 2008), the annular mode is the preferred climate response to arbitrary mechanical and thermal forcings.

However, because of the complex eddy–zonal flow interactions in the annular modes, it is still not well understood what determines the persistence of the zonal wind anomalies and the mechanism that sustains the positive eddy feedback. Observational studies found that, underneath the interactions between the eddy momentum forcing and the zonal wind anomalies, the latitudinal shift of the midlatitude jet is always accompanied by a persistent shift of the lower-flow baroclinicity. Lorenz and Hartmann (2001, 2003) through composite analysis found that when the jet shifts poleward (equatorward),

Corresponding author address: Yang Zhang, School of Atmospheric Sciences, Nanjing University, 22 Hankou Road, Nanjing, Jiangsu 210093, China.
E-mail: yangzh@alum.mit.edu

DOI: 10.1175/JAS-D-11-0214.1

the maximum baroclinicity of the lower-level flow, which is the eddy source region, also moves poleward (equatorward) of its time-mean position, indicating that there could exist a baroclinic mechanism that sustains the positive eddy–zonal flow feedback. Robinson (2000) argues that the shift of the lower-level baroclinicity with the jet can enhance the persistence of the annular modes through a positive feedback loop; that is, the shift of the baroclinicity results in the latitudinal shift of the eddy generation, which causes a shift of the eddy momentum forcing on the zonal flow and further enhances the zonal wind anomalies. However, the variation of the lower-level baroclinicity with the jet shift appears to contradict the conventional ''negative feedback'' between baroclinic eddies and the zonal flow baroclinicity. As shown in the eddy life cycle or eddy equilibrium studies (Gutowski et al. 1989; Zurita-Gotor and Lindzen 2007), baroclinic eddies always act to reduce the flow baroclinicity and make the flow more barotropic. Thus, the mechanism that sustains the latitudinal shift of lower-level baroclinicity with the zonal jet is a key process for understanding the positive eddy feedback in the annular modes and needs further study.

Several processes have been suggested for the persistent displacement of the lower-level baroclinicity in the annular modes. Robinson (1996, 2000) suggested that surface friction, which acts to increase the baroclinic wind shear, can play an important role in maintaining the positive feedback between the eddies and the zonal wind anomalies. Chen and Plumb (2009) further showed that, by keeping the strong vertical wind shear at lower levels, stronger surface friction can result in stronger positive eddy feedback in the annular modes, although the persistence of the annular mode is reduced as a direct result of the enhanced frictional damping on the zonal winds. Robinson (2006) and Gerber and Vallis (2007) suggested that the positive eddy feedback depends on the meridional wave propagation in the upper levels. If midlatitude eddies can propagate away from the center of the jet and be absorbed near the flanks of the jet, the resulting Eliassen–Palm (EP) flux convergence will exhibit a local maximum near the jet core and drive a thermally indirect residual circulation, which can act to reinforce the baroclinicity in the latitude of the jet core and extend the persistence of the eddy-driven jet.

A recent study by Zhang et al. (2009) found that the maintenance of the lower-level baroclinicity strongly depends on the critical line distribution of the energy-containing eddies. Different distributions of the lower-level critical line result in different regime behaviors on how the eddies shape the lower-level zonal flow baroclinicity. The critical line, by definition, is the region where zonal wind is equal to the phase speed of the eddies. Linear instability studies (Pedlosky 1987; Lindzen et al. 1980; Lindzen and Barker 1985) showed that the baroclinic eddies are generated in the lower levels where the critical line is located. Eddy equilibration studies also showed that, in the lower levels, it is near the critical line that the eddy heat flux is strongest, characterized by strong eddy–zonal flow interactions (Zurita and Lindzen 2001). In this study, with a simplified multilayer model, we will show that, in addition to the surface friction and the upper-level eddy propagation, the critical line distribution at lower levels can be crucial for maintaining the strong lower-level baroclinicity at the jet-core latitudes in the annular modes. This baroclinicity restoration allows for a positive feedback loop that enhances the zonal wind anomalies. Eddies with different critical line distributions respond to the zonal wind anomalies differently. For eddies with lower phase speed (low frequency) and critical lines emerging at the flanks of the jet at lower levels, their eddy thermal forcing acts to enhance the lower-level baroclinicity at the center of the jet, which results in persistent shift of the lower-level baroclinic zone in the annular modes. Our sensitivity studies further indicate that these low-phase-speed eddies can play a critical role in maintaining the annular mode–like variations of the zonal wind. Without these eddies, the zonal wind variability can shift from the latitudinal fluctuation of the jet position to a pulsing of the jet intensity.

The structure of this paper is assigned as below. Section 2 is a description of the numerical experiments carried out in the study. The sensitivities of the zonal winds' low-frequency variation to the surface friction are shown in section 3. The eddy–zonal flow interactions in the annular mode–like variations in the sensitivity runs are studied in section 4. The mechanisms through which surface friction affects the flow's low-frequency variation are investigated in section 5. A summary and discussion of the results are presented in section 6.

2. Experiment description

To better illustrate the eddy–zonal flow interactions in the annular modes, a modified β-plane quasigeostrophic (QG) channel model with interactive static stability and a simplified boundary layer parameterization is used in this study, similar to that of Solomon and Stone (2001) and Zhang et al. (2009). As shown by Gutowski (1985), the interaction between the vertical eddy heat flux and the stratification, which is neglected in conventional QG theory, could play an important role in the eddy–zonal flow interactions in the midlatitude. To overcome this major limitation of the traditional QG model, the horizontally averaged static stability in our model, instead of being specified, is allowed to evolve with time according

to the horizontally averaged thermodynamic equation (also see the appendix for the details of the model). The modified model keeps the simplicity of the traditional QG model but can simulate more realistic midlatitude dynamics.

The model has a channel length of 21 040 km, which is comparable with the length of the latitudinal belt in midlatitudes, and a channel width of 10 000 km with the baroclinic zone centered over the central half of the channel, which represents the width of the baroclinic zone over midlatitudes. Thus, the model simulates a pure midlatitude jet symmetric about the center of the channel, and does not capture the influence of spherical geometry and the subtropical jet, which may also play a role in the variability, as suggested in Lee and Kim (2003) and Vallis and Gerber (2008). To better study the relative roles of the upper- and lower-flow variations in the annular modes (e.g., the flow baroclinicity), the model is set with 17 equally spaced levels in the pressure coordinates. Similar to Zhang et al. (2009), the model in this study is integrated with a fixed surface temperature. The surface temperature difference over the baroclinic zone is 43 K, which approximates the temperature difference over the midlatitudes in winter in the Northern Hemisphere.

The surface heat flux and surface friction in the model are parameterized with the linearized bulk aerodynamic drag formula with drag coefficients c_{dt} and c_{df}, respectively, representing the strength of the processes. In the boundary layer, the turbulent vertical heat and momentum fluxes are parameterized as a vertical diffusion, the strength of which is separately controlled by the diffusion coefficients μ_s and μ_m.

In this study, the eddy–zonal flow interactions in the annular modes are investigated through the sensitivity runs to surface friction. The surface friction, as shown in Zhang et al. (2009), can strongly modify the zonal flow and the eddy activities. For the zonal flow, surface friction can directly reduce the lower-level zonal winds. Furthermore, as suggested in Robinson (2000) and further studied by Chen and Plumb (2009), surface friction, by keeping the lower-level baroclinicity, can enhance the eddy feedback in the annular modes but reduce the time scale of the zonal wind anomalies. On the other hand, previous studies indicate that surface friction also strongly modifies the eddy activities in a few ways. In addition to acting as a sink of eddy kinetic energy, surface friction affects the inverse energy cascade (Held 1999) and acts as an important factor that determines the length scale of the energy-containing eddies. As a result, the spatial distribution of the critical line (Zhang et al. 2009) and the eddy–zonal flow interactions can be modified with the variation of the surface friction as well. To clearly understand the variations of the eddy and the zonal flow in the sensitivity runs, in this study only the surface friction on the eddies is varied in the sensitivity runs. The surface friction on the zonal flow is kept unchanged, which is different from the experiments in Robinson (2000) and Chen and Plumb (2009). Thus, any variation of the zonal flow variability in the sensitivity runs is purely eddy-induced.

More precisely, the surface stress τ_m in the frictional damping in the model is modified as follows:

$$\tau_m = -c_{df}\rho_s\mathbf{v}^* - c_{dm}\rho_s[\mathbf{v}], \tag{1}$$

where $\mathbf{v} = (-\psi_y, \psi_x)$; square brackets denote the zonal average and an asterisk denotes the deviation from the zonal average (eddy components). In the standard run, which is designed to simulate an annular mode–like variation of the zonal wind, we set $c_{df} = c_{dm} = 0.012$ m s^{-1}. In the sensitivity runs, c_{df} is varied from 0.012 to 0.036 m s^{-1} with an increment of 0.004 m s^{-1}, while fixing $c_{dm} = 0.012$ m s^{-1} at surface. Each simulation in the sensitivity runs starts from the axisymmetric state with small-amplitude perturbations added to the axisymmetric flow at the initial moment. All of the experiments are integrated for 5000 days and the statistics are based on the last 3000 days. Variations of the zonal flow's climatology and the leading-mode variability with the surface friction are shown in the next section.

3. Time-mean state and the zonal wind variability

a. The time-mean state

Variations in the surface friction on eddies result in strong variations in the eddy activity and the eddy length scale. The eddy kinetic energy (EKE) and the averaged eddy length scale $\overline{L}_{\text{eddy}}$ in the sensitivity runs are plotted in Fig. 1. The averaged eddy length scale is defined as $\overline{L}_{\text{eddy}} = L_{\text{channel}}/\overline{k}$ and the averaged eddy zonal wavenumber $\overline{k} = \int kE(k)\,dk/\int k\,dk$, where L_{channel} is the length of the channel and $E(k)$ is the spectral distribution of EKE with the zonal wavenumber k. To test whether $\overline{L}_{\text{eddy}}$ could be related to the Rhines scale L_β, where $L_\beta = \text{EKE}_{\text{bt}}^{1/4}/\beta^{1/2}$ and EKE_{bt} is the barotropic EKE, EKE_{bt} is also plotted in Fig. 1. The eddy activity becomes weaker under stronger frictional dissipation, consistent with the fact that surface friction is the primary sink of EKE. When $c_{df} = 0.028$ m s^{-1}, the normalized $\text{EKE}^{1/4}$ is reduced to 70% (which means that EKE is reduced to less than one-fourth of its standard run value). Further increase in the surface friction has little impact on the EKE. Variations of the barotropic EKE is similar to the total EKE, which is obviously reduced under stronger surface friction. In the regime of weak surface friction

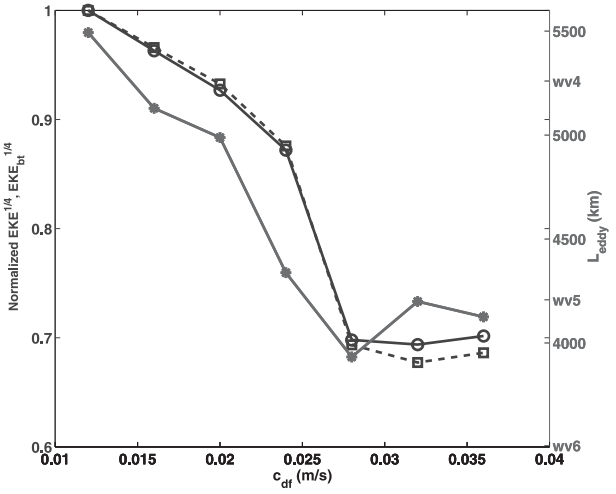

FIG. 1. Time- and domain-averaged fourth root of EKE (black solid line with open circles) and barotropic EKE (black dashed line with open squares) normalized by their corresponding values in the standard run, and the averaged eddy length scale (gray solid line with asterisks) as a function of surface friction. For eddy length scale, the corresponding zonal wavenumber is also labeled on the *y* coordinate.

(i.e., $c_{df} = 0.012$–0.020 m s^{-1}) the averaged eddy length scale is close to zonal wavenumber 4. With the stronger surface friction, the averaged eddy length scale is reduced to the length scale close to zonal wavenumber 5. The variation of $\overline{L}_{\text{eddy}}$ is highly consistent with the variation of EKE_{bt} in the regime of weak surface friction. In the regime of strong surface friction, the variation of $\overline{L}_{\text{eddy}}$ exhibits a different tendency with EKE_{bt}, with $\overline{L}_{\text{eddy}}$ slightly increased under the stronger surface friction, which implies that the upscale energy cascade may not be the dominant process that determines $\overline{L}_{\text{eddy}}$. In this parameter regime, $\overline{L}_{\text{eddy}}$ might be close to the most unstable mode[1] for the baroclinic instability (Schneider and Walker 2006).

Variations in the eddy activity and eddy length scale in the sensitivity runs are further investigated in the zonal wavenumber–phase speed covariance spectra of the eddy fluxes. Using the method similar to Randel and Held (1991),[2] we calculate the time-mean covariance spectra of $[v^*T^*]$ at 875 hPa at the center of the channel and the covariance spectra of $[u^*v^*]$ at 437.5 hPa at latitude 1000 km south of the channel center for the standard run and the $c_{df} = 0.036$ m s^{-1} run. As shown in Fig. 2, the lower-level eddy heat flux and the upper-level eddy momentum flux show similar zonal wavenumber–phase speed covariance spectra in both simulations, which indicates that the upper-level eddy momentum flux is closely related to the lower-level eddy generation. In the standard run, as shown in Figs. 2a and 2b, most of the eddy fluxes come from wavenumber 4 with a phase speed around 4 m s^{-1} and wavenumber 6 with a phase speed around 11 m s^{-1}. The distinct phase speeds for the two zonal wavenumbers also indicate that their eddy fluxes are characterized by distinct time scales. Eddies from zonal wavenumber 6 are characterized by synoptic time scales, around 3–5 days, while eddies from zonal wavenumber 4 are characterized by a broader range of time scales, 10–30 days (which are estimated from the zonal wavenumber–period cospectra analysis). In the $c_{df} = 0.036$ m s^{-1} run, as shown in Figs. 2c and 2d, the eddy fluxes mostly come from zonal wavenumbers 5 and 6 with phase speed around 10 m s^{-1}, whose characteristic time scales are all around 3–5 days. Thus, as the surface friction changes, the phase speeds and time scales of the energy-containing eddies also exhibit evident variations.

The time-mean-state zonally averaged zonal wind distributions in the sensitivity runs are displayed in Fig. 3. As surface friction on the zonal mean flow is kept unchanged in the sensitivity studies, variations of the zonally averaged flow are purely eddy-driven. As shown in Figs. 3a and 3b, in both the upper and lower levels the midlatitude jets are all located at the center of the channel and exhibit similar zonal wind strength at the jet core latitudes. Variations of the zonal winds mainly lie in the jet flanks. In the upper levels, the zonal winds exhibit weaker horizontal shear at the jet flanks as the surface friction increases. In the lower levels, as the frictional damping on baroclinic eddies is enhanced, the zonal winds are more confined to the jet center.

Compared to the zonal winds, the temperature field exhibits the structural change more clearly, especially in the lower levels. In the upper levels, as shown in Fig. 4a, the variation mainly occurs when the surface friction is sufficiently strong. With the reduced eddy activity, the strong baroclinicity in the upper levels is retained. However, in the lower levels, as shown in Fig. 4b, as the surface friction is enhanced, the meridional temperature gradients at the jet core and jet flanks show opposite variations. The latitudinal distribution of the lower-level temperature gradient exhibits clear regime behavior. When surface friction is weak (i.e., $c_{df} = 0.012$, 0.016, and 0.020 m s^{-1}), strong baroclinicity at the jet core is maintained, while the zonal flow baroclinicity at the jet

[1] A linear instability analysis, a method similar to that in Solomon and Stone (2001), has been carried out on the equilibrium states in the sensitivity runs. For all of the zonal mean states in the sensitivity runs, zonal wavenumbers 6 and 5 are the two linearly most unstable modes.

[2] To display the contribution from each zonal wavenumber, different from Randel and Held (1991), the spectra are not smoothed by any spectral window.

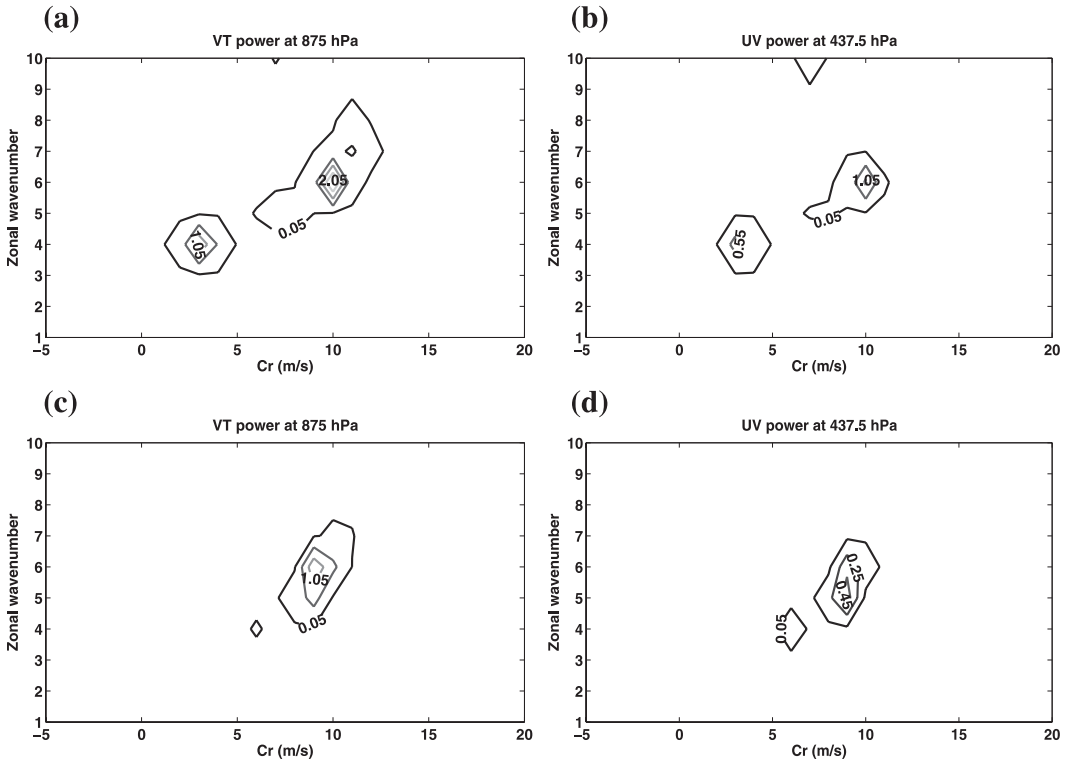

FIG. 2. Zonal wavenumber–phase speed covariance spectra of (a) $[v^*T^*]$ at 875 hPa at the center of the channel and (b) $[u^*v^*]$ at 437.5 hPa at 1000 km south of the channel center for the standard run. (c),(d) As in (a),(b), respectively, but for $c_{df} = 0.036$ m s^{-1} run. The contour interval is 0.5 K m s^{-1} ΔC_r^{-1} in (a) and (c) and 0.5 and 0.2 m^2 s^{-2} ΔC_r^{-1} in (b) and (d), where the unit phase speed interval is 1.0 m s^{-1}.

flanks is efficiently reduced. However, when the surface friction is strong, the baroclinicity at the jet center is strongly reduced and the strongest baroclinicity in the lower levels is found at the jet-flank latitudes. The different spatial variations of the lower-level flow baroclinicity cannot be simply explained by the reduction of total eddy activity. Instead, variations in the length scale of energy-containing eddies and the subsequent different spatial distributions of the eddy–zonal flow interactions, as suggested in Zhang et al. (2009), are the dominant reasons, which will be further discussed in sections 4 and 5.

b. The leading mode of variability

The leading mode of the zonal wind variability is defined by the first empirical orthogonal function (EOF) of the zonally and vertically averaged zonal wind. The principal component associated with the leading EOF is hereafter defined as UPC1. To illustrate the magnitude of the structures, the EOFs in this study are presented in units of meters per second instead of the normalized form. This is done by a regression of the anomaly data on the normalized UPC1. As the surface friction varies, the leading EOF of the zonal flow exhibits a clear transition. Figure 5 displays the leading EOFs in the runs where $c_{df} = 0.012$ and 0.036 m s^{-1}, representing the two regimes of the leading EOF in the sensitivity runs. In the regime of weak surface friction (i.e., $c_{df} = 0.012$, 0.016, and 0.020 m s^{-1}), as shown in Fig. 5a, the leading EOF represents north–south fluctuations in the position of the midlatitude jet, whose time-mean position is at the center of the channel. In all of these low friction runs, this mode can explain more than 40% of the total variance, although the dominance is reduced with enhanced surface friction. The leading EOF of the zonally averaged zonal wind in these runs is also plotted in Fig. 5c, whose structure is an equivalent barotropic dipole with maximum anomalies 1000 km (around 10° latitude) away from the center of the jet. The PC time series with this leading EOF is essentially the same as UPC1: the two time series are correlated at 0.99. The leading EOFs in the regime of relatively weak surface friction, as in Figs. 5a–c, are close to the annular modes observed in the Southern and Northern Hemispheres (Lorenz and Hartmann 2001, 2003). The second EOF of the zonally and vertically averaged zonal wind is also displayed in Fig. 5a, which exhibits a tripole pattern representing the pulsing of the jet intensity. This mode is similar to the observed second

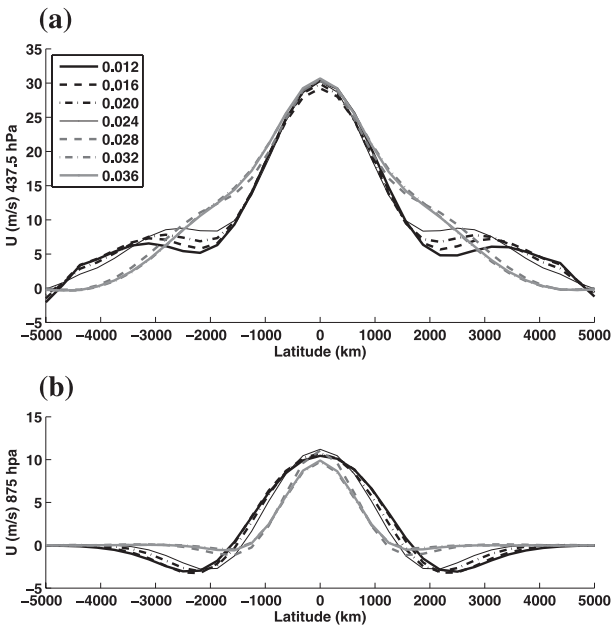

FIG. 3. Latitudinal distribution of the time-averaged and zonally averaged zonal winds at (a) 437.5 and (b) 875 hPa for different surface friction values. The latitudinal distance on the x coordinates is in kilometers, with 0 km denoting the center of the channel and positive (negative) values denoting the latitudinal distance poleward (equatorward) of the channel center.

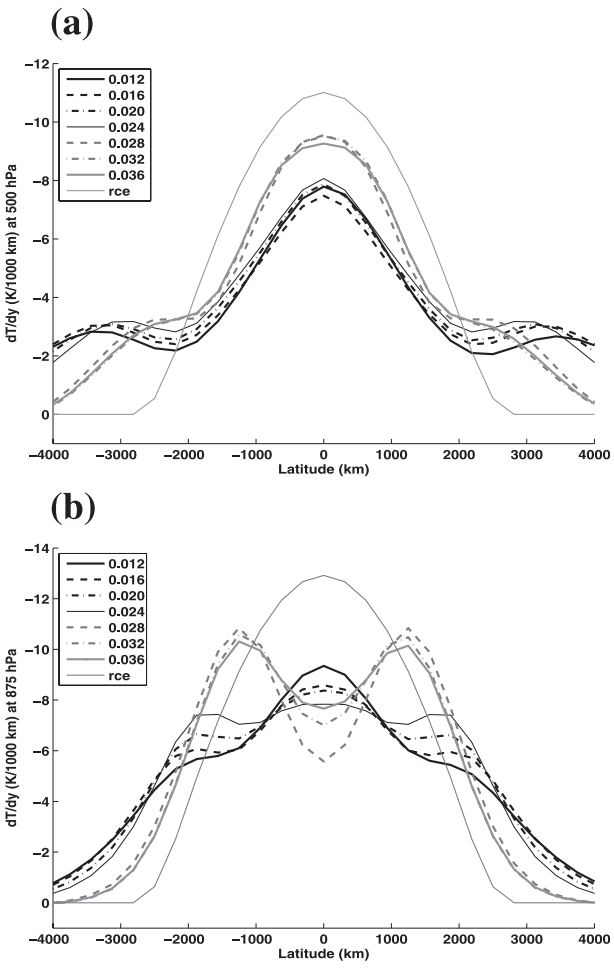

FIG. 4. Latitudinal distribution of the time-averaged and zonally averaged temperature gradient at (a) 500 and (b) 875 hPa for different surface friction values.

EOF of the zonally averaged tropospheric zonal winds in the real atmosphere as well.

As the surface friction increases, the leading EOF pattern changes. In the regime of strong surface friction (i.e., $c_{df} = 0.028$, 0.032, and 0.036 m s^{-1}), as shown in Fig. 5b, the leading mode of the zonal wind variability shifts to a pulse of the midlatitude jet, which explains more than 50% of the zonal wind variability. The leading mode of the zonally averaged zonal wind, as shown in Fig. 5d, also shows a tripole structure, representing the strengthening/weakening of the jet over the whole troposphere. For $c_{df} = 0.024$ m s^{-1}, the variability of the zonal wind behaves as a transition point of the two regimes (results not shown here).

As the variation of the zonally averaged zonal wind in the sensitivity runs is purely induced by the different surface friction on the eddy activity, an EOF analysis is also applied to the eddy forcing. From the zonal momentum equation under the β-plane quasigeostrophic approximation

$$\frac{\partial}{\partial t}[u] = -\frac{\partial}{\partial y}[u^*v^*] + f[v] - [F], \qquad (2)$$

where the residual forcing F is dominated by friction, the zonal wind in the vertical average (barotropic jet) is forced by the eddy momentum flux convergence and the surface friction. Thus, the EOF analysis is applied to $-(\partial/\partial y)[u^*v^*]$, whose leading EOFs in the sensitivity runs are displayed in Figs. 5e and 5f. The leading EOF of the eddy forcing is similar to that of the zonally averaged zonal wind, displaying the same transition as the zonal wind, with the EOF pattern varying from a dipole to a tripole structure as the surface friction increases.

The persistence of the zonal wind anomaly in the sensitivity runs is also estimated by calculating the decorrelation time scale from the autocorrelation functions of UPC1. The decorrelation time scale τ is obtained by performing a least squares fit to an exponential function $\exp(-\Delta t/\tau)$ between the autocorrelation value 1 and the threshold value $\exp(-1)$, where Δt is the lag time. The decorrelation time scale for the eddy momentum forcing is also estimated from the PC time series of its leading mode. As shown in Fig. 6, in all the simulations, the eddy

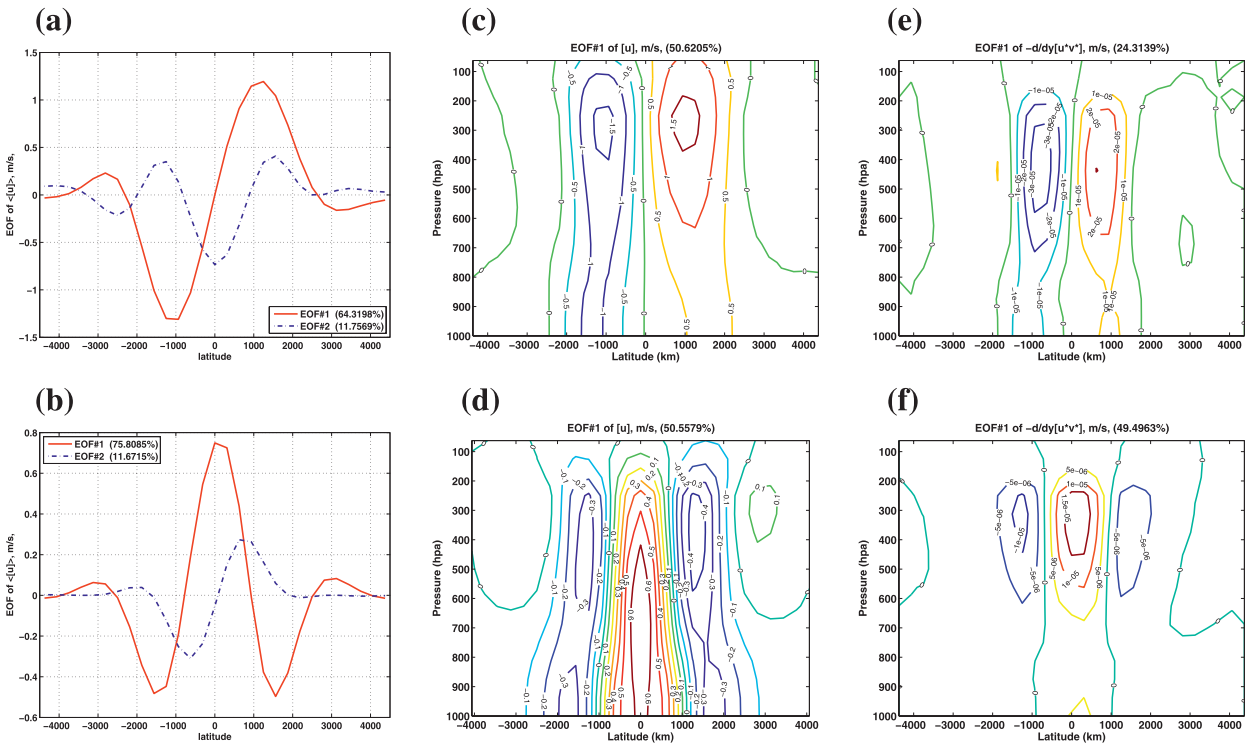

FIG. 5. The first two EOFs of zonally and vertically averaged zonal wind, the leading EOF of zonally averaged zonal wind, and the leading EOF of zonally averaged eddy forcing $-\partial/\partial y[u^*v^*]$ for (a),(c),(e) the standard run and (b),(d),(f) the $c_{df} = 0.036$ m s^{-1} run.

forcing shows a high-frequency feature, with a time scale around 2–5 days. For the zonal wind, in the regime of the weak surface friction, the zonal wind anomaly is much more persistent than the eddies, although with evident reduction in the time scale as c_{df} increases. When $c_{df} = 0.024$ m s^{-1}, the zonal wind shows high-frequency variation. In the regime of strong surface friction, the persistence of the zonal wind anomaly is evidently reduced compared to that when the surface friction is weak, although it is still more persistent than the time scale of the eddy activity. Along with the reduced persistence, the overall low-frequency variance of the zonal flow gets weaker.

Our experiments show that, as the surface friction on the eddy activity varies, both the climatology and the variability of the zonal flow show strong variations with regime behavior. An annular mode–like variation of the zonal wind can be obtained only when the surface friction on the eddies is not too strong. When the surface friction is strong, the leading mode of the zonal wind variability shifts from the north–south fluctuation of the jet position to the pulsing of the jet intensity. The eddy forcing variation shows the same transition as the zonal wind when the surface friction varies. The variations of the eddy–zonal flow interactions in the sensitivity runs are investigated in the next two sections.

4. The eddy–zonal flow interactions in the annular mode–like variations

In this section, we take the standard run ($c_{df} = 0.012$ m s^{-1}) as an example to investigate the eddy–zonal flow interactions in the annular mode–like variations. The analysis carried out in the section is also applied to the other simulations in the regime of weak surface friction in the sensitivity runs. The eddy–zonal flow

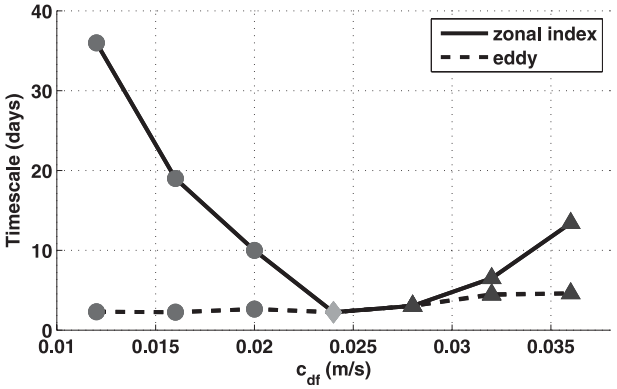

FIG. 6. The decorrelation time scales of UPC1 and eddy forcing time series as a function of surface friction. Runs with the dipole leading mode are marked with circles; runs with the leading mode representing a jet pulsing are marked with triangles.

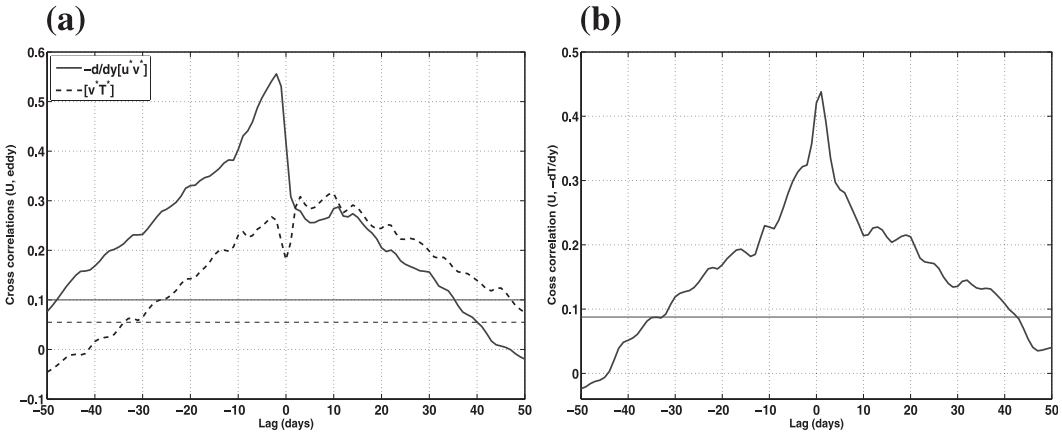

FIG. 7. Lagged cross correlations between (a) UPC1 and the time series of eddy momentum forcing (thick solid curve) and eddy heat flux (thick dashed curve) and (b) UPC1 and the time series of the second EOF (north–south shift pattern) of $-\partial[T]/\partial y$ at 875 hPa in the standard run. Positive lags denote that zonal mean zonal wind leads eddies, while negative lags denote that eddies lead the zonal mean zonal wind. The thin lines denote the corresponding values of 95% significance level, which are estimated from the autocorrelations of each time series.

interactions in those runs are found with the same features as that in the standard run, only with the strength of the eddy feedback varying with the friction.

a. The eddy feedback

As the first step to investigate the eddy–zonal flow interactions in the annular mode–like variations, similar to Lorenz and Hartmann (2001, 2003), a time series of the eddy forcing of the annular mode was calculated. We compute the eddy forcing time series by projecting the zonally and vertically averaged eddy momentum forcing in Eq. (2) onto the leading mode of the zonal wind. The strength of the eddy feedback is then evaluated by taking the cross correlation between UPC1 and the eddy forcing time series. The cross correlation in the weak surface friction simulation is shown in Fig. 7a. Consistent with the observations (Lorenz and Hartmann 2001, 2003; Rashid and Simmonds 2004) and the numerical simulations[3] (Eichelberger and Hartmann 2007; Chen and Plumb 2009), the strongest positive correlation occurs when the eddy forcing leads the zonal wind anomaly (negative lags) by around 3 days. A smaller positive correlation between them is also obtained when UPC1 leads the eddy momentum forcing and peaks around the 10-day lag, indicating a positive feedback between the zonal wind anomaly and the eddy forcing.

Although not directly apparent in Eq. (2), as suggested in Robinson (2006) and Chen and Plumb (2009), the anomalous eddy heat flux, which always indicates the anomalous eddy generation, can play an important role in the positive eddy feedback in the annular modes. Observational studies by Lorenz and Hartmann (2001) and Kidston et al. (2010) suggest that the latitudinal shift of the zonal jet is associated with the anomalous latitudinal shift of the eddy generation. Thus, an eddy heat flux index is defined to indicate the extent to which it is latitudinally displaced. The heat flux index is calculated by projecting the zonally averaged eddy heat flux onto its second EOF,[4] which is a pure latitudinal shifting mode. As the total eddy heat flux peaks at the jet-core latitude, this mode is characterized with a dipolar spatial pattern as well. The cross correlation between UPC1 and eddy heat flux index is also estimated and displayed in Fig. 7a. The shape of the cross correlation is consistent with the observations in Kidston et al. (2010). At negative lags, a positive cross correlation peaks at day −3 to −2. At day 0, the cross correlation reaches a relative minimum. At positive lags, a strong positive correlation is also sustained, which shows that, following the poleward displacement of the jet, the eddy heat flux anomaly also shifts poleward of its climatological position. At positive lags, the positive cross correlation first peaks at day 3 and then a second peak emerges around day 9, which all precede the correlation peak that between the zonal wind anomaly and the eddy momentum forcing. From the baroclinic eddy life cycle study (Simmons and Hoskins

[3] As in Chen and Plumb (2009), the strength of the eddy feedback also varies with the friction. In our sensitivity runs, the correlations are reduced with enhanced surface friction.

[4] For the zonally averaged eddy heat flux and the lower-level temperature gradient, their first EOF all represents a pulsing of their intensity associated with the eddy life cycle, whose distributions are not shown here.

1978), this feature indicates a poleward displacement of the baroclinic eddy generation along with the jet shift.

The generation of the baroclinic eddies is always strongest in the lower levels where the zonal flow baroclinicity is strong. To investigate the variation of the lower-level baroclinicity following the zonal wind anomaly, cross correlation between UPC1 and the time series of the 875 hPa zonally averaged temperature gradient $-\partial/\partial y[T]$ variation is also estimated. The time series of the temperature gradient variation is taken as the PC time series of the second EOF of the lower-level temperature gradient, which represents a latitudinal shift (taking the poleward shift as the positive phase) of the strongest baroclinic zone from the center of the channel (results not shown here). The cross correlation in Fig. 7b shows that the poleward shift of midlatitude jet is followed by a poleward shift of the lower-level baroclinicity as well, and the shift of the lower-level baroclinicity extends much longer than a single baroclinic eddy life cycle, which overcomes the baroclinicity reduction from the lower-level eddy heat flux. Thus, consistent with the observations, Figs. 7a and 7b together suggest that there could be a baroclinic mechanism that acts to maintain the latitudinal displacement of the jet. The poleward (equatorward) displacement of the eddy-driven jet, as a direct response to the anomalous eddy momentum forcing, leads to poleward (equatorward) shifts of the lower-level baroclinic zone, the generation of the eddy activity, and the eddy momentum forcing aloft. These processes together act as a positive feedback that drives the anomalous zonal wind. The whole process occurs in a few days following the jet shift. However, even after the poleward shift of the lower-level eddy heat flux, which acts to reduce the lower-level temperature gradient, the strong lower-level baroclinicity accompanied with the shifted jet is still retained and extended. This is a key process in the positive eddy–zonal flow feedbacks in the annular modes, which will be further investigated in the following subsections.

b. The persistent shift of the lower-level baroclinicity

1) THE CLIMATOLOGY VIEW

To understand the variation of the lower-level baroclinicity in the annular modes, we first investigate how the climatological baroclinicity is maintained. As shown in Zhang et al. (2009), the lower-level baroclinicity is sensitive to the critical line distribution of the energy-containing eddies, which is the region where the zonally averaged zonal wind is equal to the phase speed C_r of the eddy. In the regime of weak surface friction, as shown in Fig. 2, the eddy heat and momentum flux in the flow mostly comes from zonal wavenumbers 4 and 6, which are characterized by distinct phase speeds. Thus, the cross sections of $(U - C_r)$ and the contributions in $[v^*T^*]$ of the two zonal wavenumbers are plotted in Figs. 8a and 8b, respectively. The phase speeds of the dominant waves are calculated at each time step following Gall (1976):

$$C_r = [k(\phi_s^2 + \phi_c^2)]^{-1}\left(\phi_c\frac{\partial\phi_s}{\partial t} - \phi_s\frac{\partial\phi_c}{\partial t}\right), \qquad (3)$$

where ϕ_s and ϕ_c are the Fourier coefficients of the streamfunction in terms of sine and cosine components, respectively. The contributions from zonal wavenumbers 4 and 6 in $[v^*T^*]$ are calculated from the covariance spectra

$$\mathrm{Cov}_k(v, T) = 2\mathrm{Re}\langle\tilde{v}(k)\tilde{T}^{\mathrm{conj}}(k)\rangle, \qquad (4)$$

where $k = 4$ and 6, $\tilde{v}$ is the Fourier coefficient of v, and $\tilde{T}^{\mathrm{conj}}$ is the conjugate of the Fourier coefficient of the temperature.

As shown in Figs. 8a and 8b, eddies from the two zonal wavenumbers display different spatial distributions of the critical line and the meridional eddy heat flux. For zonal wavenumber 4, with the slower phase speed, the lower-level critical line disappears from the center of the jet and shifts to the flank regions. For zonal wavenumber 6, however, $U - C_r$ shows clear vertical variation, with the critical line emerging around 850 hPa at the center latitudes of the jet. With different critical line distributions, the eddy heat fluxes from the two zonal wavenumbers also display different spatial distributions. As shown in Figs. 8a and 8b, the eddy heat flux always peaks around the lower-level critical line. For zonal wavenumber 6, the eddy heat flux peaks at the center latitude of the jet around the critical level (around 850 hPa). As the critical line of zonal wavenumber 4 shifts away from the center of the jet, the eddy heat flux from zonal wavenumber 4 shows double peaks at the critical latitudes in the lower level. The spatial distribution of the eddy heat flux shows that the generation of the eddy activity is strongly related to the lower-level critical line distribution. This is reasonable given that baroclinic instability essentially can be understood as a critical layer behavior (Lindzen et al. 1980; Pedlosky 1987; Zurita and Lindzen 2001). It is near the critical line that the eddy–zonal flow interactions are strongest. Our analysis shows that the location of the lower-level critical line is consistent with the position of the eddy source region.

With different spatial distributions of the eddy heat flux, zonal wavenumbers 4 and 6 play different roles in maintaining the lower-level baroclinicity. Cross sections of their components in the eddy thermal forcing

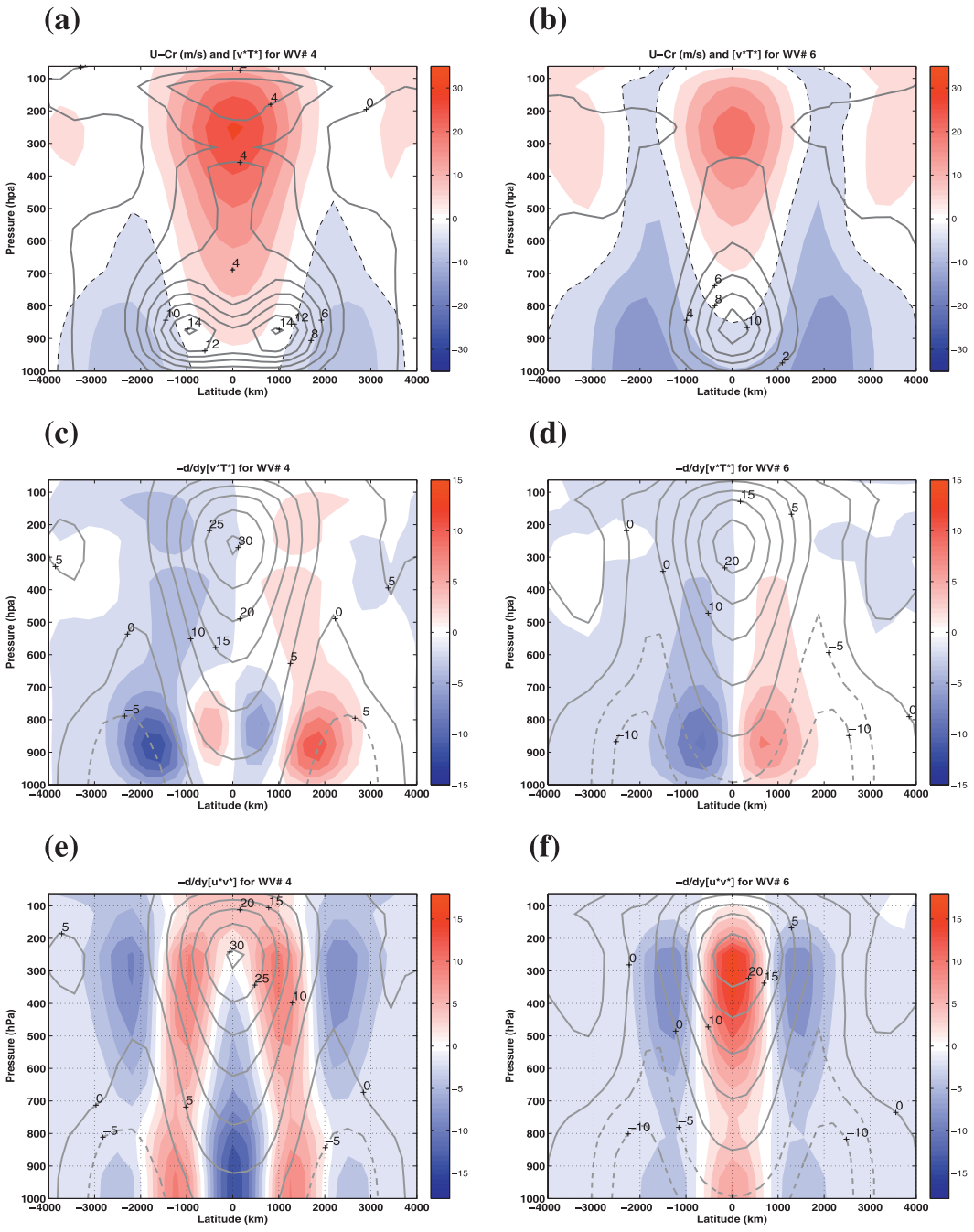

FIG. 8. Cross sections of the time-mean $U - C_r$ (color shaded) and the components in $[v^*T^*]$ (gray solid contours) for zonal wavenumbers (a) 4 and (b) 6 in the standard run; cross sections of the zonal wavenumbers (c) 4 and (d) 6 components in the time-mean $-(\partial/\partial y)[v^*T^*]$ (color shaded); and the zonal wavenumbers (e) 4 and (f) 6 components in the time-mean $-(\partial/\partial y)[u^*v^*]$ (color shaded). In all panels, the blue shaded region denotes negative values. In (a) and (b), the contour interval is 2 K m s^{-1} for $[v^*T^*]$ and 5 m s^{-1} for $U - C_r$ with the zero contour plotted in dashed curves. The contour interval is 2×10^{-6} K s^{-1} in (c) and (d) and 2×10^{-6} m s^{-2} in (e) and (f). In (c)–(f), the corresponding distributions of $U - C_r$ are also plotted as gray curves, with negative values plotted as dashed curves.

$-(\partial/\partial y)[v^*T^*]$ are displayed in Figs. 8c and 8d, respectively. The eddy thermal forcing from zonal wavenumber 6 is confined to the central latitudes of the jet, with net cooling in the lower latitudes and net warming in the higher latitudes, which acts to reduce the lower-level baroclinicity at the center of the jet. For zonal wavenumber 4, as the eddy activity is centered at the jet-flank regions, its eddy thermal forcing acts to reduce the

baroclinicity near the jet flanks but acts to enhance the lower-level baroclinicity at the jet center, which offsets the baroclinicity reduction of the eddy thermal forcing from zonal wavenumber 6. Because of the competing effects between zonal wavenumbers 4 and 6, as shown in Fig. 4b, the lower-level baroclinicity remains strongest at the jet center but is efficiently reduced at the jet flanks, a mechanism similar to that suggested in Zhang et al. (2009).

Cross sections of the eddy momentum forcing $-(\partial/\partial y)[u^*v^*]$ from zonal wavenumbers 4 and 6 are also plotted in Figs. 8e and 8f. Over most of the troposphere, the eddy momentum forcing from zonal wavenumber 4 acts to accelerate the jet at the flanks but decelerate the jet at the center, almost opposite to the eddy momentum forcing of zonal wavenumber 6 in Fig. 8f. The jet deceleration at the center by wavenumber 4 is stronger in the lower level,[5] which could also help increase the vertical shear of the zonal wind. The different eddy momentum forcings of the two wavenumbers on the zonal flow are consistent with the different distributions of their lower-level eddy source regions. As in Vallis (2006), the eddy momentum forcing on the zonal jet is strongly governed by the eddy generation in the lower levels, the schematics of which for the two wavenumbers are illustrated in Fig. 9. For zonal wavenumber 6, as shown in Figs. 9a and 9b, the eddy source region is at the center of the jet. Thus the wave energy of wavenumber 6 propagates away from the center of the jet, especially after reaching the upper levels, with the momentum flux acting to accelerate the jet at the center. For zonal wavenumber 4, however, as the eddy source regions are at the flanks of the jet as in Fig. 9c, its momentum flux at the center of the jet is in the direction opposite to zonal wavenumber 6.

Above analysis showed that, with distinct phase speeds and critical line distributions, eddies from zonal wavenumbers 4 and 6 are characterized by different eddy source regions and different eddy forcings on the zonal flow. As summarized in Fig. 9, eddy heat and momentum fluxes of the two zonal wavenumbers exhibit distinct impacts on the zonal baroclinicity and barotropic jet. This implies that the two eddies might play different roles in the annular mode–like variations of the zonally averaged zonal wind, which will be further investigated in the next subsection.

[5] In the upper levels, with strong $U - C_r$, waves can propagate meridionally throughout the jet center with little decay. Thus, the two groups of eddies from wavenumber 4, which are generated at the jet flanks and propagate into the jet from opposite directions, can cancel each other at the jet center, resulting in weaker jet deceleration there.

2) THE SHIFT OF THE LOWER-LEVEL BAROCLINIC ZONE IN THE ANNULAR MODES

To understand the different roles of the eddies from zonal wavenumbers 4 and 6 in the annular modes, similar to Fig. 7a, cross correlations between UPC1 and the time series of the eddy forcing from the two zonal wavenumbers are plotted in Fig. 10. The shape of the cross correlation for wavenumber 6 displays a positive feedback between the eddy momentum forcing and the zonal wind anomaly. The eddy heat flux from zonal wavenumber 6 exhibits a clear positive peak when the zonal wind anomaly leads the heat flux for around 3 days, which indicates a persistent latitudinal shift of the eddy generation. For zonal wavenumber 4, at positive lags, the cross correlation between UPC1 and the eddy momentum forcing becomes negative, which indicates that the eddy momentum forcing from wavenumber 4 acts to decay the anomalous zonal wind after the latitudinal jet shift; however, the correlation coefficients are weak. For zonal wavenumber 4, because its eddy heat flux exhibits different latitudinal and vertical distribution from the total eddy heat flux, it is thus not appropriate to project onto the leading mode of the total flux to obtain its time series. The role of the eddy heat flux from zonal wavenumber 4 in the annular modes is investigated in the regression analysis.

To diagnose the effect of the zonal wind anomalies on the eddies from zonal wavenumbers 4 and 6, we do time-lagged regressions of the anomalous eddy heat flux, eddy heat flux convergence, and eddy momentum convergence on UPC1. As shown in the previous section, after a zonal wind anomaly has peaked, the eddy response lasts longer than an eddy life cycle. To isolate that part of eddy forcing, we regress the eddy flux and the eddy forcings on UPC1, with UPC1 leading by 10 days. As shown in Fig. 11, the eddy components from the two zonal wavenumbers show different response to the poleward shift of the midlatitude jet. For zonal wavenumber 6, as shown in Fig. 11d, the eddy heat flux response shows a dipole pattern, while the eddy heat flux from zonal wavenumber 4 exhibits a tripole pattern, as in Fig. 11a. Compared to their time-mean state, the response of the eddy heat flux from the two zonal wavenumbers all indicates a poleward shift to their time-mean positions. Consistent with the eddy heat flux response, the response of the eddy heat flux convergence from the two zonal wavenumbers indicates a poleward shift to their time-mean position as well. Thus, as shown in Figs. 11b and 11e, along with the zonal wind anomaly, the eddy thermal forcing from zonal wavenumber 4 acts to maintain a poleward shift of the baroclinic zone, while the eddy thermal forcing from zonal wavenumber 6 acts to offset the baroclinic zone

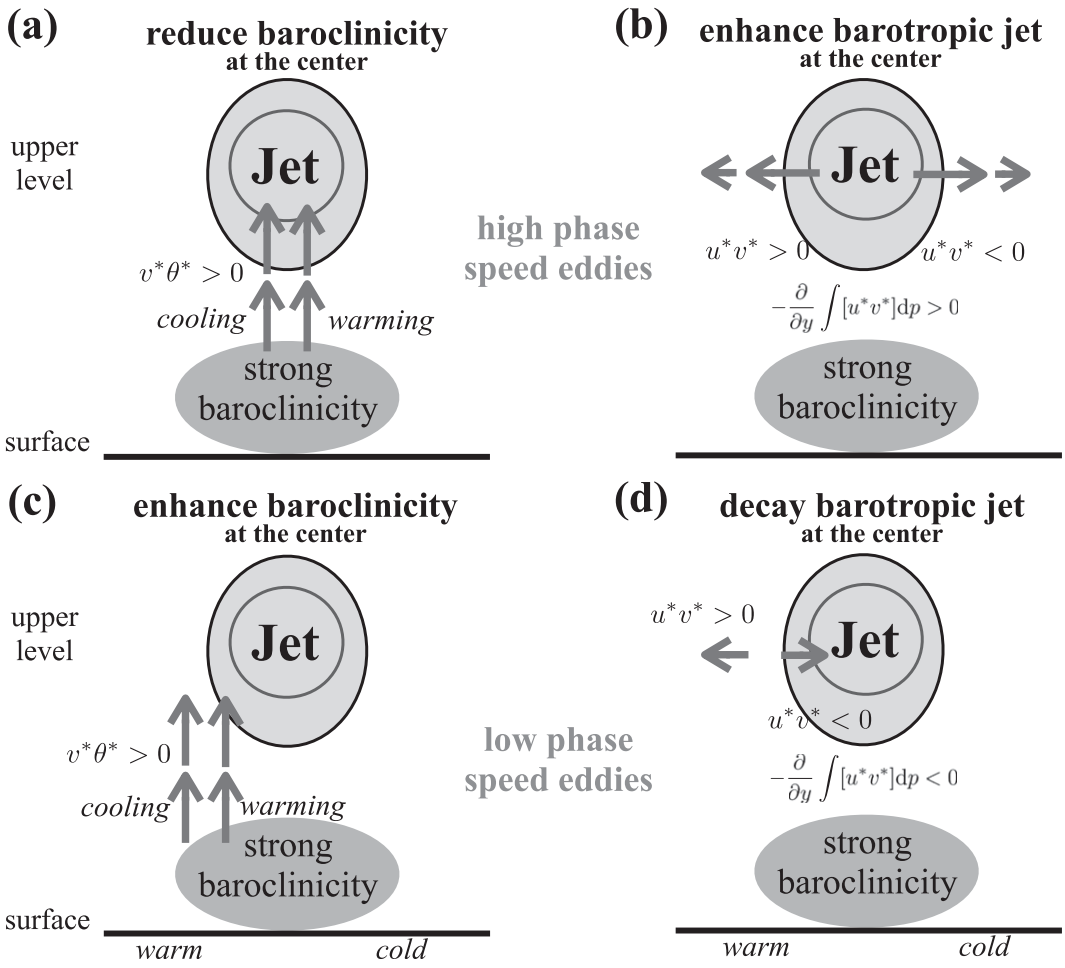

FIG. 9. Diagrams showing the impacts of eddy heat and momentum fluxes on the zonal flow baroclinicity and zonal winds at the center of the jet for zonal wavenumbers (a),(b) 6 and (c),(d) 4 in the standard run. Arrows denote the propagation of baroclinic wave activity. In (c) and (d), because of space limits, only the eddies generated at one flank of the jet are illustrated. High-phase-speed eddies as zonal wavenumber 6 generated at the center of jet act to reduce the baroclinicity and enhance the barotropic jet. Low-phase-speed eddies as zonal wavenumber 4 generated at the flanks of the jet act to enhance the baroclinicity at the jet center and decay the barotropic jet.

shift. The eddy momentum convergence from zonal wavenumber 6, consistent with the cross correlations in Fig. 10b, acts to enhance the zonal wind anomaly, while zonal wavenumber 4 exhibits a different response pattern, which at the jet-core latitudes mainly acts to decay the zonal wind anomaly. The different response pattern of the eddy forcing from zonal wavenumber 4 also helps explain the low correlations between UPC1 and the eddy forcing time series in Fig. 10a.[6]

The above regression analysis illustrates the competing forcings of zonal wavenumbers 4 and 6 on the zonal mean zonal wind and lower-level baroclinicity. To compare the relative importance of zonal wavenumbers 4 and 6 on the zonal flow, time-lagged regressions are also applied on the net anomalous eddy forcings of the two waves. As shown in Figs. 11g and 11h, zonal wavenumber 4 dominates the eddy thermal forcing in the lower levels. At 875 hPa, the net eddy thermal forcing in Fig. 11h shows a similar pattern to the wavenumber 4 in Fig. 11b, acting to enhance the poleward shift of the baroclinic zone. For the net eddy momentum forcing on the zonal flow, Fig. 11i shows that forcings from zonal wavenumber 6 are dominant, especially in the upper levels, acting to enhance the zonal wind anomalies.

[6] The results of the regression analysis are also supported by the composites of the eddy heat flux, eddy forcings, and critical line distributions of the two zonal wavenumbers in the positive and negative phases of the annular modes. The most significant variation between the two phases is the latitudinal shift of the whole system.

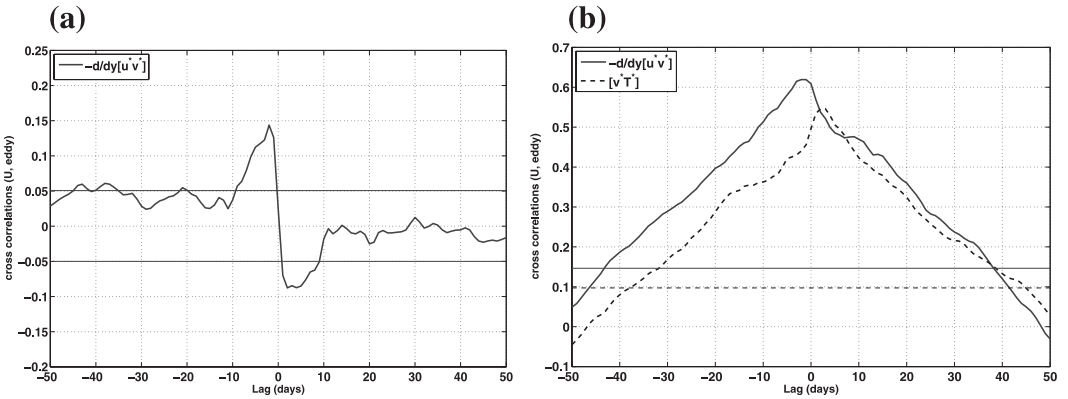

FIG. 10. As in Fig. 7a, but for the components in $-(\partial/\partial y)[u^*v^*]$ and $[v^*T^*]$ from zonal wavenumbers (a) 4 and (b) 6. In (a), because the vertical and latitudinal structure of $[v^*T^*]$ for zonal wavenumber 4 is not coherent with the leading mode, its time series and cross correlation with UPC1 are not estimated.

The relative roles of zonal wavenumbers 4 and 6 in sustaining the latitudinal shift of the lower-level baroclinicity are further investigated in Fig. 12. Instead of the eddy thermal forcing $-\partial/\partial y[v^*T^*]$, which represents the eddy heating rate on the zonal flow, the 875-hPa $\partial^2/\partial y^2[v^*T^*]$ from the two zonal wavenumbers are projected on the shifting mode (second EOF) of the 875-hPa $-\partial/\partial y[T]$. This term represents the eddy differential heating on the zonal low, which is a direct forcing exerting on the lower-level baroclinicity. The cross correlations between the time series of 875-hPa $-\partial/\partial y[T]$ and the eddy thermal forcings from the two waves are plotted in Fig. 12. The cross correlations again display the competing effects of zonal wavenumbers 4 and 6 in the latitudinal shift of the lower-level baroclinicity. Furthermore, for the eddy forcing from zonal wavenumber 4, there is a strong positive correlation peaking around day −2, indicating that the poleward shift of the lower-level baroclinicity is greatly driven by zonal wavenumber 4. For zonal wavenumber 6, a negative correlation peaks around day 3, showing a poleward shift of the eddy thermal forcing as well as the eddy generation for zonal wavenumber 6 following the latitudinal shift of the lower-level baroclinicity. The magnitudes of the correlations in Fig. 12 also indicate that the negative feedback from zonal wavenumber 6 for the lower-level baroclinicity is efficiently offset by zonal wavenumber 4; thus, the poleward shift of the lower-level baroclinic zone is extended.

Our analysis in Fig. 12 suggests that the poleward shift of the lower-level baroclinicity is greatly attributed to the poleward displacement of the eddy thermal forcing from zonal wavenumber 4. Then what is the process that drives the poleward displacement of zonal wavenumber 4? A study by Zhang et al. (2009) showed that for low-phase-speed eddies like zonal wavenumber 4, they are characterized by the lower-level critical lines at the jet flanks. The climatology and transient behaviors of the eddy heat flux from these eddies can be organized by their lower-level critical line variations. In the standard run in Fig. 8a, the climatological distribution of the eddy heat flux for zonal wavenumber 4 is shown highly related to the critical line distribution. To test the relation between the latitudinal shifts of the eddy thermal forcing and their critical line variations in the annular modes, lagged cross correlations are also calculated between the time series of $U - C_r$ and eddy thermal forcing for zonal wavenumber 4. Before we estimate the cross correlations, an EOF analysis is applied to the $U - C_r$, whose leading EOF is also a dipolar pattern (result not shown here). A lagged cross correlation between PC1 of $U - C_r$ and UPC1 is calculated and displayed in Fig. 13, in which autocorrelations of PC1 and UPC1 are also plotted for comparison. The cross correlation peaks at day 0, with the peak correlation as high as 0.84, indicating that the latitudinal shift of $U - C_r$ mostly occurs simultaneously with the zonal wind anomalies. The high correlation between PC1 and UPC1 also indicates that the variations of $U - C_r$ are mainly associated with the zonal wind anomalies, although, compared to the autocorrelations of PC1 and UPC1, the phase speed C_r also exhibits fast and small-amplitude variations. The time series of the eddy thermal forcing from zonal wavenumber 4 is estimated by projecting on the leading EOF of $U - C_r$. The lagged cross correlation between the time series of $U - C_r$ and the eddy thermal forcing in Fig. 13 exhibits strong positive correlations as well with a strong positive peak at day 0, showing that the latitudinal shifts of the eddy thermal forcing for zonal wavenumber 4 are highly correlated to its critical line variations. This high cross correlation suggests that the transient variations of zonal wavenumber 4 in the annular modes may also be organized by the latitudinal shift of the critical line.

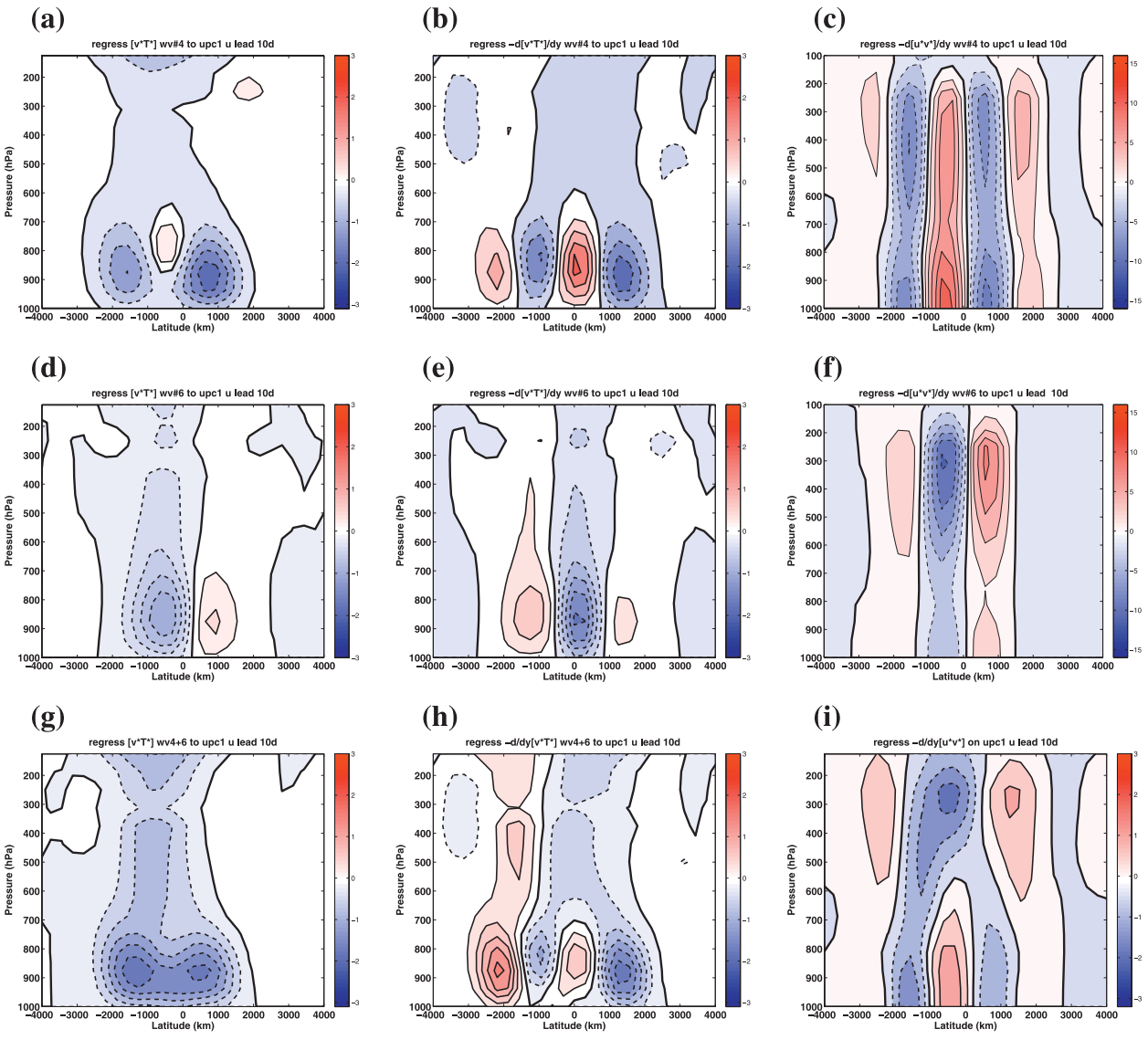

FIG. 11. Anomalous zonally averaged (a),(d),(g) eddy heat flux, (b),(e),(h) eddy heat flux convergence, and (c),(f),(i) eddy momentum flux convergence from zonal wavenumbers 4, 6, and 4 + 6 together, respectively, regressed on UPC1 in the standard run. UPC1 leads by 10 days. Positive (negative) values are plotted in solid (dashed) contours. Zero lines are plotted in thick solid contours.

Our analysis in this section shows that, following the anomalous zonal wind, eddy forcings from zonal wavenumbers 4 and 6 exhibit different responses. Zonal wavenumber 4 dominates the eddy thermal forcing in the lower level, acting to enhance the lower-level baroclinicity at the jet core, while zonal wavenumber 6 dominates the eddy momentum forcing, acting to enhance the zonal wind anomalies. Our analysis also suggests a baroclinic mechanism through which zonal wavenumbers 4 and 6 work together maintaining the annular mode–like variations. Following the anomalous zonal wind and the associated critical line variation, the anomalous eddy thermal forcing from zonal wavenumber 4 drives and sustains a latitudinal shift of the lower-level baroclinic zone, which results in the anomalous eddy generation of zonal wavenumber 6. The anomalous eddy momentum forcing from zonal wavenumber 6 acts as a positive eddy feedback that enhances and extends the zonal wind anomalies in the annular modes.

5. Transition in the leading mode of the zonal wind variability

As shown in Fig. 5, with the enhanced surface frictional damping on the eddies, the leading mode of the zonal wind variability shifts from a north–south fluctuation of

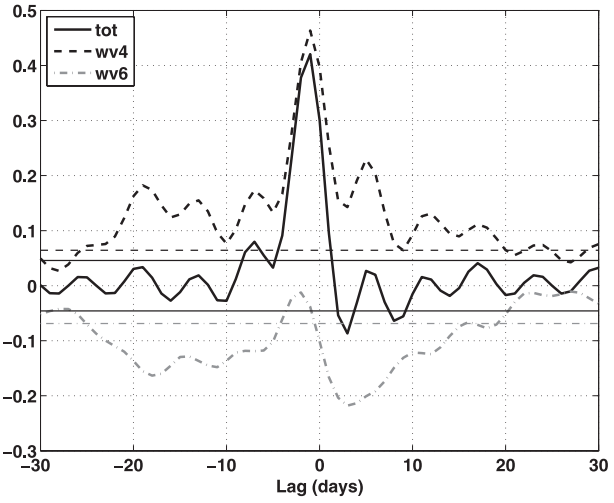

FIG. 12. Lagged cross correlations between the time series of 875 hPa $-\partial[T]/\partial y$ and total eddy thermal forcing $\partial^2/\partial y^2[v^*T^*]$ (thick solid curve), and eddy forcing from zonal wavenumber 4 (thick dashed curve) and 6 (thick dash-dotted curve). Positive lags indicate that zonal flow leads the eddy. The thin lines denote the corresponding values of 95% significance level.

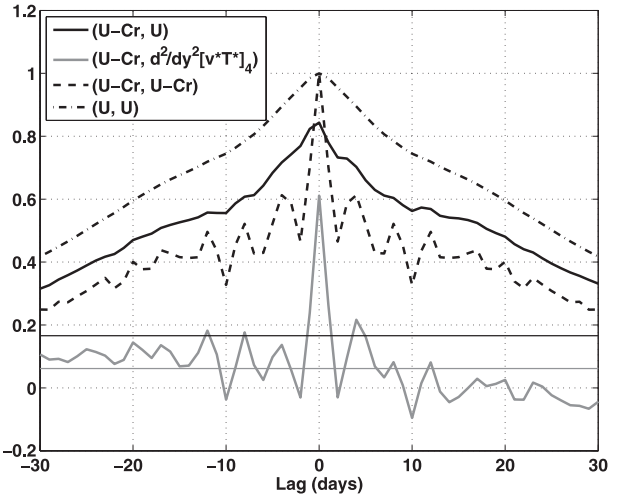

FIG. 13. Lagged cross correlations between PC1 of $U - C_r$ for zonal wavenumber 4 and UPC1 (thick black curve), and times series of eddy thermal forcing $\partial^2/\partial y^2[v^*T^*]$ from zonal wavenumber 4 (thick gray curve). Positive lags denote that $U - C_r$ leads the eddy and U. The thin lines denote the corresponding values of 95% significance level. Autocorrelations of UPC1 and PC1 of $U - C_r$ for zonal wavenumber 4 are also shown with a dash-dotted and a dashed curve, respectively.

the jet position to a strengthening/weakening of the jet intensity. The increase of the surface friction results in reduction in the eddy energy and the eddy length scale, which are the two candidate reasons for the transition of the leading mode. As shown in Fig. 1, the domain-averaged EKE decreases to less than one-fourth of the value in the standard run. The zonal wavenumber–phase speed covariance spectra in Figs. 2c and 2d show that, for strong surface friction, the eddy heat/momentum fluxes are mostly the contributions from zonal wavenumbers 5 and 6, which are eddies characterized by high phase speeds. The critical line and the eddy flux distributions of these energy-containing eddies are similar to the zonal wavenumber 6 in the standard run in Figs. 8b,d,f. Their momentum forcing acts to enhance the upper-level jet, while the eddy thermal forcing acts to reduce the lower-level baroclinicity (results not shown here). In the flow, the low-phase-speed eddies as the zonal wavenumber 4 in the standard run are missing.

To understand the relative roles of the variations in the strength and the length scale of the eddies in the transition of the zonal wind variability, a filtered simulation is carried out. In the filtered run, instead of increasing the surface friction, a fast Fourier transform (FFT) filter is applied to the streamfunction in the model to remove the eddies with length scale greater than zonal wavenumber 5. Thus, in the filtered run simulation, the eddy energy is allowed to be as active as in the standard run but, similar to the strong friction runs, the larger-scale eddies, which are always characterized with lower phase speeds, are prevented from playing any roles in the system. The model is also integrated for 5000 days in the simulation with the statistics based on the last 3000 days.

The climatological spatial distributions of the zonal mean zonal wind and baroclinicity in the filtered run are plotted in Figs. 14a and 14b to compare with the standard and the $c_{df} = 0.036$ m s^{-1} runs. As shown in Fig. 14a, in both upper and lower levels, the latitudinal distributions of the zonal wind in the filtered run are closer to the strong surface friction run. The most dramatic variations in the time-mean state are the lower-level baroclinicity. At the jet-center latitudes, as shown in Fig. 14b, the lower-level baroclinicity is strongly reduced, whereas at the jet flanks the baroclinicity is strong and enhanced. Such spatial distribution is also more similar to the distribution in the $c_{df} = 0.036$ m s^{-1} run. The lower-level baroclinicity distribution in the filtered run can be understood from the eddy heat flux distribution. In the filtered run, without the larger-scale eddies, most of the eddy energies are confined to zonal wavenumber 6, whose critical line and eddy heat flux distributions are shown in Fig. 14c. The eddy heat flux from zonal wavenumber 6 is much stronger than the strong friction run but exhibits similar spatial distribution. The eddy heat flux, consistent with its critical line distribution, is centered at the jet-core latitudes and thus acts to strongly reduce the zonal flow baroclinicity there. This also helps us

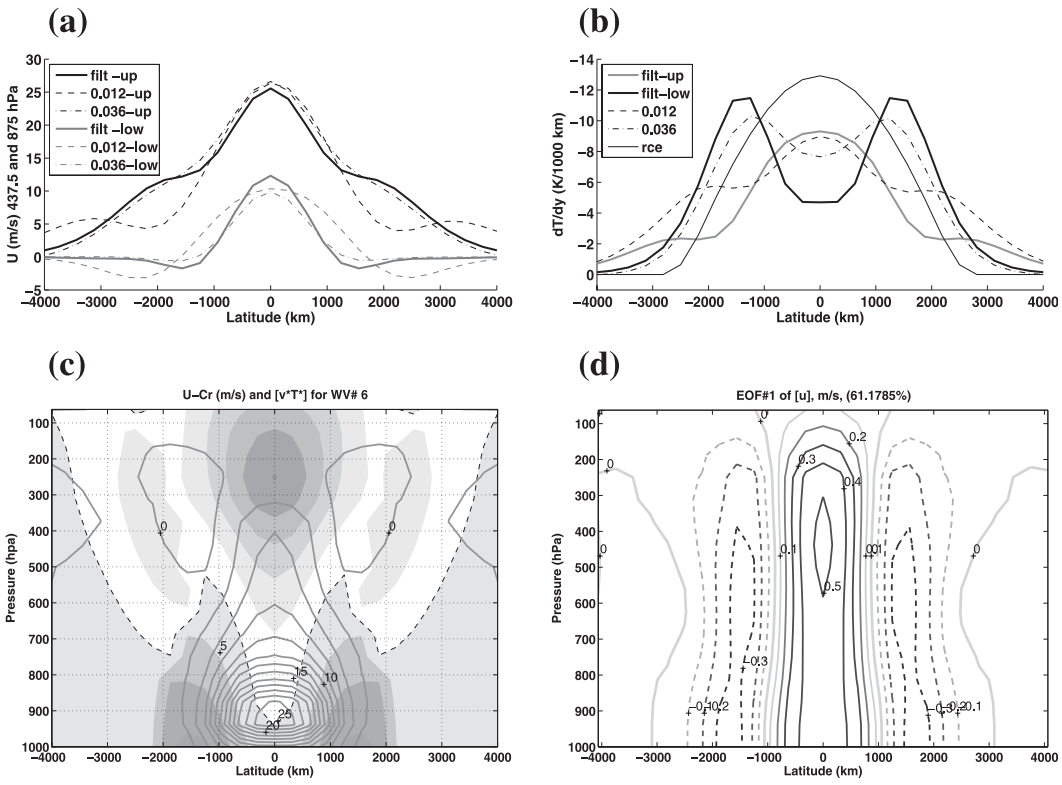

FIG. 14. Latitudinal distributions of time- and zonal mean (a) upper- (437.5 hPa) and lower-level (875 hPa) zonal wind and (b) lower-level meridional temperature gradient in the filtered run simulation. The corresponding distributions in the standard and $c_{df} = 0.036$ m s^{-1} runs are also plotted for comparisons. In (b), the upper-level temperature gradient in the filtered run is plotted as well. (c) As in Fig. 8a, but for components from zonal wavenumber 6, and (d) the leading EOF of the zonally averaged zonal wind in the filtered run simulation.

understand why with the stronger eddy heat flux in the filtered run, the lower-level baroclinicity at the jet-center latitudes is more efficiently reduced compared to that in the strong surface friction run. Compared to the standard run, this variation also implies the crucial role that low-phase-speed eddies can play in maintaining the strong lower-level baroclinicity at the jet-center latitudes. With the strong variations in the equilibrium state, the leading mode of the zonal wind variability, as shown in Fig. 14d, also shifts to a tripole pattern. The filtered run simulation indicates that the absence of the larger-scale eddies as well as the corresponding eddy forcings on the zonal flow are the dominant reasons for the transition in the zonal wind variability.

Above analysis all indicate that the preferentially damping of the low-phase-speed eddies with enhanced surface friction plays a dominant role in the transition in the leading mode of the zonal wind variability. The high-phase-speed eddies as zonal wavenumbers 5 and 6 are characterized by a critical layer at the jet-core latitude in the lower troposphere. When they are the only dominant eddies in the flow, the lower-level baroclinicity is efficiently reduced by eddy mixing. Then, different from the standard run, there are no eddies like zonal wavenumber 4 that can enhance the lower-level baroclinicity within the jet in the time-mean state as well as in the latitudinal shifts of the eddy-driven jet. Thus, our sensitivity study suggests a baroclinic mechanism for the transition in the leading mode of the zonal wind variability. The transition of the leading mode also implies that the low-phase-speed eddies as zonal wavenumber 4 in the standard run may play a crucial role in maintaining the annular mode–like variations of the zonal wind.

6. Summary and discussion

Using a modified multilayer QG channel model, we have shown that eddies with different length scales and phase speeds (time scales) play different roles in sustaining the annular mode–like variations of the mid-latitude jet. We argue that these differences can be explained in terms of different critical line structures experienced by high- and low-phase-speed eddies. For

eddies with higher phase speed (synoptic eddies), the eddy generation region is always located at the jet-core latitudes, whose propagation out of the jet acts to reinforce the jet and drives the zonal wind anomalies associated with the annular modes. For low-phase-speed eddies (low-frequency eddies), which are always characterized by larger length scale, their critical line distributions in the lower levels and their generation regions are away from the center of the jet. As a result, their thermal forcing on the zonal flow enhances the lower-level baroclinicity, which offsets the baroclinicity reduction from the high-phase-speed eddies and sustains the persistent displacement of the lower-level baroclinic zone in the annular modes. Our study further suggests a baroclinic mechanism through which the high-phase-speed and the low-phase-speed eddies work symbiotically to maintain the annular mode–like variations. That is, following the anomalous zonal wind and the resulting critical line variations, the anomalous eddy thermal forcing from the low-phase-speed eddies drives a latitudinal shift of the lower-level baroclinic zone, which results in a latitudinal displacement of the eddy generation of the synoptic eddies. The anomalous eddy momentum forcing from the synoptic eddies further enhances the zonal wind anomalies. The above processes work together, establishing a positive feedback loop that extends the persistence of the annular modes.

We noted, for the direct momentum forcing on the zonal flow, that the role that the low-phase-speed eddies played in our study is consistent with the observed ''low-frequency'' eddies or ''residual'' eddies (Lorenz and Hartmann 2001) in the southern annular mode (SAM), which acts as a negative or oscillating effect to the anomalous zonal winds. Our study implies that their different behavior from the high-frequency eddies might be attributed to the different spatial distributions of the critical line and the generation regions of these eddies. More importantly, our study shows that these low-phase-speed eddies can play crucial roles in maintaining the strong lower-level baroclinicity at the jet core latitudes, which is a key character for the self-maintaining jet as suggested in Robinson (2006) and Vallis and Gerber (2008). By sustaining a self-maintaining jet during the jet shift, the low-phase-speed eddies can eventually help extend the persistence of the zonal wind anomalies. Thus, in addition to the enhanced residual circulation driven by the convergence of the upper-level eddy momentum flux, our study suggests another process that can act to enhance the lower-level baroclinicity in the annular modes. Furthermore, our study suggests that whether the eddy-driven jet is self-maintained may also depend on the vertical/meridional distribution of the critical line for the energy-containing eddies, a factor better simulated in the multilayer model compared to the conventionally used two-layer model.

The importance of the low-phase-speed eddies in the annular mode–like variations is further illustrated in the sensitivity studies. When the surface friction on baroclinic eddies is increased, the leading mode of the zonal wind variability can shift from a latitudinal fluctuation of the jet position to a pulsing of the jet intensity. Further analysis suggests that the transition of the leading mode can be attributed to the fact that the low-phase-speed eddies are selectively damped by the enhanced surface friction. As the frictional damping on the eddy activity is enhanced, the averaged eddy length scale becomes smaller and featured with higher phase speeds. Thus, at lower levels, a critical layer appears at the jet core latitudes, where, like a negative feedback, the baroclinicity is efficiently reduced by the eddy mixing. There is no component like the low-phase-speed eddies that acts to maintain the lower-level baroclinicity. Under this critical line distribution, the zonal wind variability is dominated by jet pulsing. The role played by the low-phase-speed eddies in our model in maintaining the lower-level baroclinicity in the annular modes is consistent with the very recent observational study by Blanco-Fuentes and Zurita-Gotor (2011), in which they also found that the low-frequency eddies, in contrast to the synoptic eddies, contribute to the low-frequency latitudinal shift of the zonal flow baroclinicity along with the SAM. Our sensitivity study further suggests that these low-frequency eddies may be crucial in establishing the positive eddy feedback in the annular modes. The sensitivity runs also indicate that, in addition to the barotropic factors (i.e., the influence of the subtropical jet; Eichelberger and Hartmann 2007; Barnes and Hartmann 2011), the transition of the leading mode of the zonal wind variability can be purely eddy-induced and driven through a baroclinic mechanism. The applications of this baroclinic mechanism to understanding the persistence of the annular modes in the real atmosphere and the sophisticated GCMs (Gerber et al. 2008) and how this mechanism can be modified given the zonal structure of the westerly jet (Barnes and Hartmann 2010) and the presence of stationary eddies (Luo et al. 2007) in the Northern Hemisphere are topics for future studies.

Acknowledgments. We thank the two anonymous reviewers for their constructive comments and suggestions, which led to an improvement of the manuscript. This study was supported by the National Natural Science Foundation of China under Grants 41005028 and 40730953. GC was supported by the US NSF Grant AGS-1064079.

APPENDIX

Model Description

In our β-plane multilevel quasigeostrophic channel model, the variables are defined in gridpoint space. The horizontal resolution of the model is 330 km in both zonal and meridional directions. The model has 17 equally spaced levels. As shown by Solomon (1997) and Solomon and Stone (2001), this horizontal and vertical resolution is appropriate to simulate the eddy dynamics. In addition, an FFT filter is used on the streamfunction to remove the smallest-scale eddies. In this study, the channel length and the width of the baroclinic zone of the model are set representing the midlatitude situations of the real atmosphere. Sensitivity tests show that the main conclusions and mechanisms proposed in this study always hold for moderate variations in the width of the baroclinic zone (i.e., from half to twice the current setting).

In the model, the potential vorticity equation, including diabatic heating and boundary layer dissipation, is integrated:

$$\frac{\partial q}{\partial t} = -J(\psi, q) - f_o \frac{\partial}{\partial p}\frac{QR}{spc_p} + \mathbf{k}\cdot\nabla\times\mathbf{F},$$

where p is the pressure, f_o is the Coriolis parameter at the center of the channel, R is the ideal gas constant, c_p is the specific heat of the air, $s = -(R/p)(p/p_o)^{R/c_p}(\partial/\partial p)\overline{\theta}^{xy}$ is the static stability parameter, and ψ is the geostrophic streamfunction; also, $\mathbf{F}$ denotes the frictional dissipation and the heating term Q has two contributors: radiative–convective heating $Q_{\rm rad}$ and the thermal diffusion in the boundary layer $Q_{\rm dif}$. Potential vorticity $q = \nabla^2\psi + f_o + \beta y + (\partial/\partial p)(f_o^2/s)(\partial\psi/\partial p)$.

One difference between this model and traditional QG models is that the horizontally averaged potential temperature and static stability, instead of being specified, are allowed to evolve with time according to the equation

$$\frac{\partial}{\partial t}\overline{\theta}^{xy} = -\frac{\partial}{\partial p}\overline{\omega^*\theta^*}^{xy} + \frac{\overline{Q_{\rm rad}+Q_{\rm dif}}^{xy}}{c_p}\left(\frac{p_o}{p}\right)^{R/c_p}, \quad \text{(A1)}$$

where $\overline{(\cdots)}^{xy}$ means averaged horizontally. More descriptions of this modification can be found in Zhang et al. (2009) and Zhang and Stone (2010). Since we still use horizontal uniform stratification, adding Eq. (5) does not break the QG scaling. The horizontal variation of the stratification is still assumed small and neglected, which, as shown in observations and numerical studies (Zurita-Gotor and Vallis 2009), is a good approximation for midlatitude climate.

Radiative–convective heating and thermal diffusion in the boundary layer are parameterized as in Zhang et al. (2009). Radiative–convective heating in the model is parameterized by the Newtonian cooling form, with the baroclinic zone confined over the central half of the channel. At the surface, a 43-K surface air temperature difference is set over the channel, which approximates the midlatitude surface temperature difference in winter in the Northern Hemisphere. In the stratosphere, the potential temperature gradient of the target state is one-tenth of that in the troposphere and of the opposite sign. For thermal diffusion in the boundary layer, the drag coefficient c_{dt} for surface heat flux and the vertical thermal diffusion coefficient μ_s for vertical turbulent heat flux in the boundary layer are taken to be 0.03 m s^{-1} and 5 m^2 s^{-1}, respectively, as in Zhang et al. (2009).

The parameterization of friction is analogous to thermal diffusion $\mathbf{F} = g(\partial\tau_m/\partial p)$, where τ_m is the shear stress and is parameterized by a linearized bulk aerodynamic drag at the surface as defined in Eq. (1) and vertical diffusion in the boundary layer:

$$\tau_m = \nu_M(p)\rho^2 g\frac{\partial \mathbf{v}}{\partial p}, \quad \text{(A2)}$$

where

$$\nu_M(p) = \mu_m\left(\frac{p}{p_o}\right)^3 \quad \text{(A3)}$$

and $\mu_m = 5$ m^2 s^{-1}. In this study, only the shear stress by geostrophic component is considered.

REFERENCES

Barnes, E., and D. Hartmann, 2010: Dynamical feedbacks of the southern annular mode in winter and summer. *J. Atmos. Sci.,* **67,** 2320–2330.

——, and ——, 2011: Rossby wave scales, propagation and the variability of eddy-driven jets. *J. Atmos. Sci.,* **68,** 2893–2908.

Blanco-Fuentes, J., and P. Zurita-Gotor, 2011: The driving of baroclinic anomalies at different timescales. *Geophys. Res. Lett.,* **38,** L23805, doi:10.1029/2011GL049785.

Chen, G., and R. Plumb, 2009: Quantifying the eddy feedback and the persistence of the zonal index in an idealized atmospheric model. *J. Atmos. Sci.,* **66,** 3707–3720.

Eichelberger, S., and D. Hartmann, 2007: Zonal jet structure and the leading mode of variability. *J. Climate,* **20,** 5149–5163.

Feldstein, S., and S. Lee, 1998: Is the atmospheric zonal index driven by an eddy feedback? *J. Atmos. Sci.,* **55,** 3077–3086.

Gall, R., 1976: A comparison of linear baroclinic instability theory with the eddy statistics of a general circulation model. *J. Atmos. Sci.,* **33,** 349–373.

Gerber, E., and G. Vallis, 2007: Eddy–zonal flow interactions and the persistence of the zonal index. *J. Atmos. Sci.,* **64,** 3296–3311.

——, L. Polvani, and D. Ancukiewicz, 2008: Annular mode time scales in the Intergovernmental Panel on Climate Change Fourth Assessment Report models. *Geophys. Res. Lett.,* **35,** L22707, doi:10.1029/2008GL035712.

Gutowski, W. J., 1985: Baroclinic adjustment and the midlatitude temperature profiles. *J. Atmos. Sci.,* **42,** 1735–1745.

——, L. E. Branscome, and D. Stewart, 1989: Mean flow adjustment during life cycles of baroclinic waves. *J. Atmos. Sci.,* **46,** 1724–1737.

Hartmann, D., and F. Lo, 1998: Wave-driven zonal flow vacillation in the Southern Hemisphere. *J. Atmos. Sci.,* **55,** 1303–1315.

Held, I., 1999: The macroturbulence of the troposphere. *Tellus,* **51,** 59–70.

Kidston, J., D. Frierson, J. Renwick, and G. Vallis, 2010: Observations, simulations, and dynamics of jet stream variability and annular modes. *J. Climate,* **23,** 6186–6199.

Lee, S., and H. Kim, 2003: The dynamical relationship between subtropical and eddy-driven jets. *J. Atmos. Sci.,* **60,** 1490–1503.

Limpasuvan, V., and D. Hartmann, 2000: Wave-maintained annular modes of climate variability. *J. Climate,* **13,** 4414–4429.

Lindzen, R. S., and J. Barker, 1985: Instability and wave overreflection in stably stratified shear flow. *J. Fluid Mech.,* **151,** 189–217.

——, B. Farrell, and K.-K. Tung, 1980: The concept of wave overreflection and its application to baroclinic instability. *J. Atmos. Sci.,* **37,** 44–63.

Lorenz, D., and D. Hartmann, 2001: Eddy–zonal flow feedback in the Southern Hemisphere. *J. Atmos. Sci.,* **58,** 3312–3327.

——, and ——, 2003: Eddy–zonal flow feedback in the Northern Hemisphere winter. *J. Climate,* **16,** 1212–1227.

Luo, D., T. Gong, and Y. Diao, 2007: Dynamics of eddy-driven low-frequency dipole modes. Part III: Meridional displacement of westerly jet anomalies during two phases of NAO. *J. Atmos. Sci.,* **64,** 3232–3248.

Pedlosky, J., 1987: *Geophysical Fluid Dynamics*. 2nd ed. Springer-Verlag, 710 pp.

Randel, W. J., and I. M. Held, 1991: Phase speed spectra of transient eddy fluxes and critical layer absorption. *J. Atmos. Sci.,* **48,** 688–697.

Rashid, H., and I. Simmonds, 2004: Eddy–zonal flow interactions associated with the Southern Hemisphere annular mode: Results from NCEP-DOE reanalysis and a quasi-linear model. *J. Atmos. Sci.,* **61,** 873–888.

Ring, M., and R. Plumb, 2007: Forced annular mode patterns in a simple atmospheric general circulation model. *J. Atmos. Sci.,* **64,** 3611–3626.

——, and ——, 2008: The response of a simplified GCM to axisymmetric forcings: Applicability of the fluctuation–dissipation theorem. *J. Atmos. Sci.,* **65,** 3880–3898.

Robinson, W. A., 1996: Does eddy feedback sustain variability in the zonal index? *J. Atmos. Sci.,* **53,** 3556–3569.

——, 2000: A baroclinic mechanism for the eddy feedback on the zonal index. *J. Atmos. Sci.,* **57,** 415–422.

——, 2006: On the self-maintenance of midlatitude jets. *J. Atmos. Sci.,* **63,** 2109–2122.

Schneider, T., and C. C. Walker, 2006: Self-organization of atmospheric macroturbulence into critical states of weak nonlinear eddy–eddy interactions. *J. Atmos. Sci.,* **63,** 1569–1586.

Simmons, A. J., and B. J. Hoskins, 1978: The life cycles of some nonlinear baroclinic waves. *J. Atmos. Sci.,* **35,** 411–431.

Solomon, A. B., 1997: The role of large-scale eddies in the nonlinear equilibration of a multi-level model of the mid-latitude troposphere. Ph.D. thesis, Massachusetts Institute of Technology, 234 pp.

——, and P. H. Stone, 2001: Equilibration in an eddy resolving model with simplified physics. *J. Atmos. Sci.,* **58,** 561–574.

Thompson, D., and J. Wallace, 2000: Annular modes in the extratropical circulation. Part I: Month-to-month variability. *J. Climate,* **13,** 1000–1016.

Vallis, G. K., 2006: *Atmospheric and Oceanic Fluid Dynamics*. Cambridge University Press, 745 pp.

——, and E. Gerber, 2008: Local and hemispheric dynamics of the North Atlantic Oscillation, annular patterns and the zonal index. *Dyn. Atmos. Oceans,* **44,** 184–212.

Zhang, Y., and P. Stone, 2010: Baroclinic eddy equilibration under specified seasonal forcing. *J. Atmos. Sci.,* **67,** 2632–2648.

——, ——, and A. Solomon, 2009: The role of boundary layer processes in limiting PV homogenization. *J. Atmos. Sci.,* **66,** 1612–1632.

Zurita, P., and R. Lindzen, 2001: The equilibration of short Charney waves: Implications for potential vorticity homogenization in the extratropical troposphere. *J. Atmos. Sci.,* **58,** 3443–3462.

Zurita-Gotor, P., and R. Lindzen, 2007: Theories of baroclinic adjustment and eddy equilibration. *The Global Circulation of the Atmosphere: Phenomena, Theory, Challenges,* T. Schneider and A. Sobel, Eds., Princeton University Press, 22–46.

——, and G. Vallis, 2009: Equilibration of baroclinic turbulence in primitive equation and quasigeostrophic models. *J. Atmos. Sci.,* **66,** 837–863.